Exploring the Environment of a Young Circumstellar Disk System

Rebecca Krall

ABSTRACT

I discuss the spectral energy distribution (SED) of the star PDS 144C, in regards to whether it is a member of the PDS 144 system. Looking at the data, I come to the conclusion that it is not a member of the system. Additionally, I perform point spread function (PSF) subtraction on the southern member of the system, PDS 144S, in an attempt to better resolve the disk and determine basic disk properties.

1. INTRODUCTION

Circumstellar disks contain particulate material and gas, and orbit stars at different phases during their life cycles. Planetary systems, asteroids, and comets are believed to form from circumstellar disks around young stars (Zuckerman 2001). The disks around main sequence stars are the remnants of the star formation process, with the majority of the original matter forming the star. Circumstellar disks dissipate from around young stars in approximately 3 to 10 million years, so there is a narrow window of time in which details of the disk can be observed. These disks can be detected from looking at the spectral energy distributions of stars. Instead of only the typical blackbody radiation of a star, the spectral energy distribution also includes excess infrared radiation, due to circumstellar disk dust particles reradiating absorbed optical and ultraviolet starlight (Zuckerman 2001). Though disks can be detected by looking at spectral energy distributions, direct imaging is necessary to determine their location and geometry. However, direct imaging is often difficult because in most cases the disk is obscured by the direct light from the star, and there is also self-shadowing.

Circumstellar disks usually form in binary or higher order multiple systems (Monin et al. 2007), so studying systems with these disks is necessary to understand planet formation. In a binary system, it is possible for the whole system to be encircled by a circumbinary disk, in addition to the individual stars having circumstellar disks (Monin et al. 2007). One example of a binary system with two circumstellar disks is PDS 144, composed of Herbig Ae stars separated by $5.4''$ (Vieira et al. 2003). The northern star is surrounded by an edge-on disk, and the southern member has substantial amounts of circumstellar dust (Perrin et al. 2006). However, the disk around 144S is obscured by the direct light from the star (Perrin et al. 2006). PDS 144C, located between the northern and southern star, is thought to be a potential third member of the system because it appears to have jets (Grady et al. 2009). This paper details the determination of whether the central star is a part of the system, and the obtainment of better resolution of the disk around 144S.

I describe the data and results for both questions in §2, and present the conclusions in §3.

2. DATA ANALYSIS AND RESULTS

To perform the data analysis, we have Hubble Space Telescope images taken at optical to near-infrared wavelengths with the ACS and NICMOS cameras. The ACS data are from 2006, and include images taken with the F555W and F814W filters with the Wide Field Camera. The NICMOS data are comprised of images taken in 2006 with the F110W and F160W filters using the NIC1 camera, and with the F205W filter and NIC2 camera. Additionally, we have NICMOS data from 2008 taken with the POL0S filter set and NIC1 camera, and with the POL0L filter set and NIC2

camera.

2.1. PDS 144C Photometry

I measure the photometry of PDS 144C using the standard technique of aperture photometry as a first step in determining whether it is a part of the system. This is accomplished by writing a Python program to measure the flux at each wavelength. First, I find the exact location of the star in each image by giving a small square of area that includes the star to a 2-D Gaussian fitting program, also written in Python, and using the resulting center values as the location of the star. The image is corrected for nonzero background next, by finding the mean of the pixels in an annulus around the star, and subtracting this mean from the image. When choosing this annulus, I do not include the diffraction spikes of PDS 144S, which pass near 144C in some images, except for the POL0L image because the diffraction spike passes through the star. Subsequently, the radius of the best signal to noise ratio is determined by iterating over each radius in pixel increments, summing the counts within in that radius, and dividing by the noise inside that radius. I estimate the noise in each radius as the standard deviation of the pixels in the annulus multiplied by the square root of the number of pixels inside that radius, plus the photon noise calculated as the square root of the signal divided by the exposure time.

The counts in the best signal to noise radius are converted to flux in Janskys by using the FITS file header keywords. The PHOTFLAM keyword (inverse sensitivity) which has units of $ergs \cdot cm^{-2} \cdot \mathring{A}^{-1} \cdot electron^{-1}$ or $ergs \cdot cm^{-2} \cdot \mathring{A}^{-1} \cdot DN^{-1}$ is multiplied by the PHOTPLAM keyword (the pivot wavelength of the filter) in units of Angstroms, and by the counts, which have units of electrons/s or DN/s. This gives the flux in units of $ergs \cdot cm^{-2} \cdot s^{-1}$. To convert to Janskys, this result is multiplied by PHOTPLAM$\cdot 10^5/(2.998) Jy \cdot cm^2 \cdot s/(erg \cdot \mathring{A})$.

Since only a portion of the star's light is included in the best signal to noise radius, I perform a correction for the aperture size. I create a model of the point spread function of a star, taken with the same filter and camera, with Tiny Tim[1], and compute the correction factor as the fraction of the model PSF's intensity which is within the chosen aperture. Finally, the flux for each star is multiplied by the inverse of the corresponding correction factor.

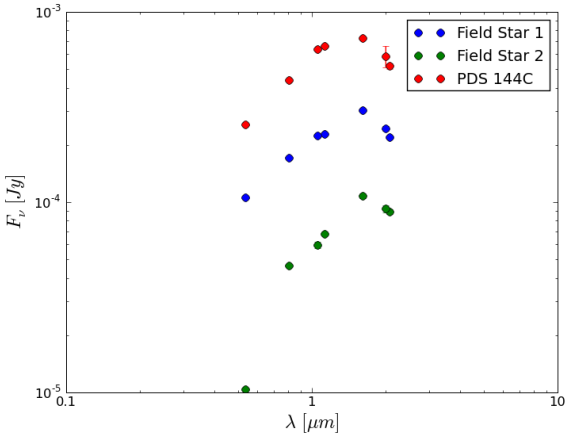

Fig. 1.— SEDs for Field Stars 1 and 2, and PDS 144C.

The uncertainty on the flux is the fractional error of the signal (noise/signal) summed with the fractional error of PHOTFLAM in quadrature, multiplied by the flux. The online NICMOS handbook gives the fractional PHOTPLAM error for the F110W, F160W, and F205W filters, while no other errors are available. I estimate the fractional error on the filters for which a value was not given as 1%. This seems reasonable given the values of the other filters. Comparing the fractional error on the signal to the fractional error in PHOTPLAM illustrates that the error in PHOTPLAM is the major source of error in the results.

In addition to measuring the photometry of PDS 144C, I measure the photometry of two background stars, Field Star 1 ($\alpha = 15^h49^m15.9^S$, $\delta = -26°00'50.8''$), and Field Star 2 ($\alpha = 15^h49^m16.0^S$, $\delta = -26°00'51.7''$) near PDS 144S. The photometry results are shown in Table 1, and the spectral energy distributions in Figure 1.

2.2. PDS 144C Spectral Type

The SED of PDS 144C is then compared to

[1]http://www.stsci.edu/software/tinytim/tinytim.html

TABLE 1
MEASURED FLUXES

Filter	PDS 144C mJy	PDS 144S mJy	Field Star 1 mJy	Field Star 2 mJy
F555W	0.2570 ± 0.0026	16.0400 ± 0.1606	0.1056 ± 0.0011	0.0104 ± 0.0001
F814W	0.4365 ± 0.0044	46.3281 ± 0.4634	0.1717 ± 0.0017	0.0463 ± 0.0005
POL0S	0.6359 ± 0.0093	31.2073 ± 0.3148	0.2238 ± 0.0047	0.0596 ± 0.0025
F110W	0.6609 ± 0.0090	144.0850 ± 1.5716	0.2293 ± 0.0038	0.0683 ± 0.0017
F160W	0.7284 ± 0.0113	532.5464 ± 3.7306	0.3048 ± 0.0049	0.1080 ± 0.0028
POL0L	0.5862 ± 0.0737	486.8454 ± 4.8733	0.2451 ± 0.0068	0.0922 ± 0.0042
F205W	0.5201 ± 0.0174	871.3806 ± 3.8377	0.2195 ± 0.0037	0.0891 ± 0.0025

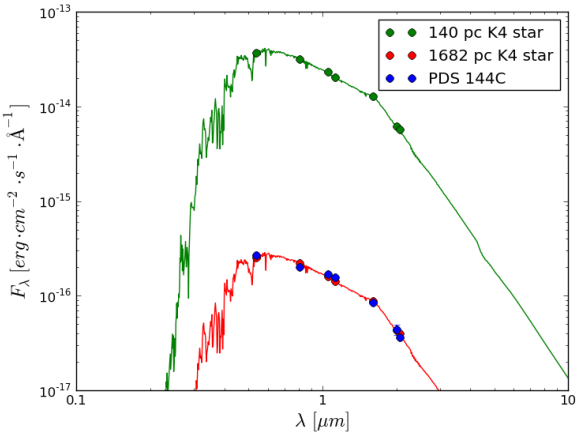

Fig. 2.— SEDs for PDS 144C and a K4 main sequence star at 140 and 1682 parsecs.

model SEDs of main-sequence stars scaled to be at 140 parsecs, the assumed distance of the system. The model SEDs are obtained from the pysynphot Python package. The comparison is accomplished by finding the reduced χ^2 value between the PDS 144C fluxes and the corresponding fluxes of the model stars using seven degrees of freedom. Then, to reduce the χ^2 values, I multiply the distance of each model star by the square root of the average ratio of the flux for that star to the flux of PDS 144C at each wavelength, since the flux of a star depends on the inverse square of the distance. The distance of PDS 144C is modified from the assumed 140 parsecs as a result of this process. For the modified distances, the lowest reduced χ^2 value, 28.6, is for a K4 main sequence star at 1682 ± 120 pc (see Fig. 3). The high χ^2 values are probably due to the flux uncertainties of PDS 144C being low.

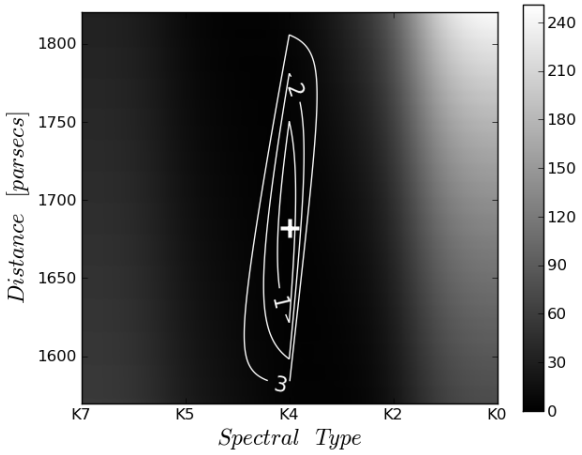

Fig. 3.— Photometry fit of PDS 144C to model main sequence stars. The χ^2 results are plotted against distance and spectral type, with interpolation between the discrete spectral types. I normalize the best-fit $\chi^2 = 1$, and plot contours of $\Delta\chi^2 = 1$, 2, and 3. A distance of 1682 pc is the best-fit distance.

2.3. *PSF Subtractions*

To attempt to resolve the disk around PDS 144S at the available wavelengths, I perform PSF subtraction on the images to reduce the starlight. Tiny Tim model PSFs are created for each im-

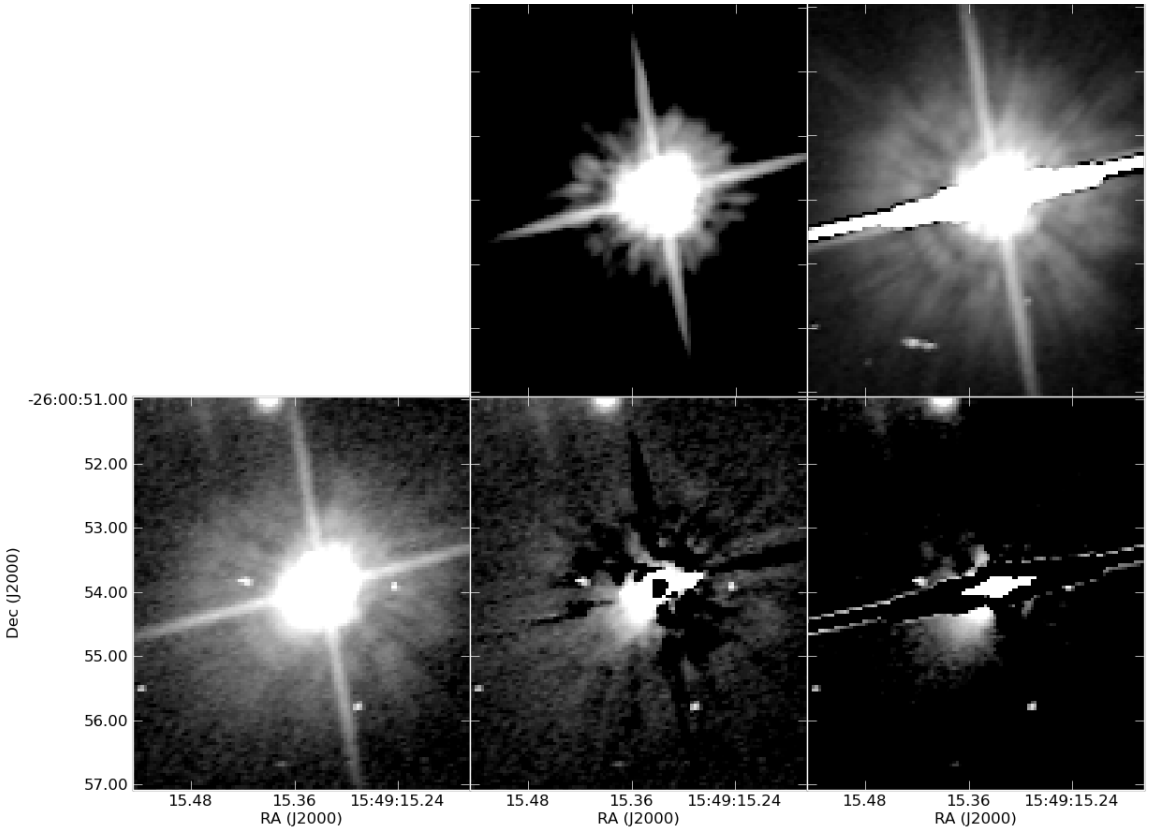

Fig. 4.— PSF subtraction results for the F555W image. The leftmost picture is the unsubtracted image, followed by the Tiny Tim PSF above its subtraction, and the field star PSF and subtracted image. The PSFs are shown multiplied by the factor that was found to produce the best subtraction. I subtract the median value off of all the images, display them at the same scale, and rotate them so that north is up. These practices are followed in the remaining PSF subtraction images.

age, with each model PSF having the same camera and filter as the image, and a power law spectrum that corresponds to the spectrum of PDS 144S at wavelengths without infrared excesses. The registration of the image with the PSF is done in IDL with Image Display Paradigm 3. I write a Python program to find the PSF multiplicative factor which gives the best subtraction. I find this factor by iterating through constants and minimizing the sum of squares of the image pixels minus the PSF image pixels multiplied by that constant. PSF subtraction on images taken with the F110W and F160W filters using the Tiny Tim PSFs and PSFs on hand do not show a clear disk, so I pursue more PSFs.

I search the Hubble archive for all stars taken with the F110W and F160W filters and their respective cameras. The coordinates of these stars are entered into the VizieR archive to obtain their 2MASS magnitudes. To determine which PSFs are the best match, I multiply the flux of each star in the J band by its exposure time, as a measure of depth, and plot this against its $J-H$ color. The Hubble archive is again searched to retrieve the images of those stars whose points on the plot are closest to that of PDS 144S, and have a clear point spread function. I use these images to do PSF subtraction on the data images, and the results are shown in (show these?). The resulting subtractions do not show anything besides noise, which leads to the conclusion that the disk cannot be resolved at these wavelengths with these data. For the short exposure images taken with F555W and F814W, I use Tiny Tim PSFs and a field star.

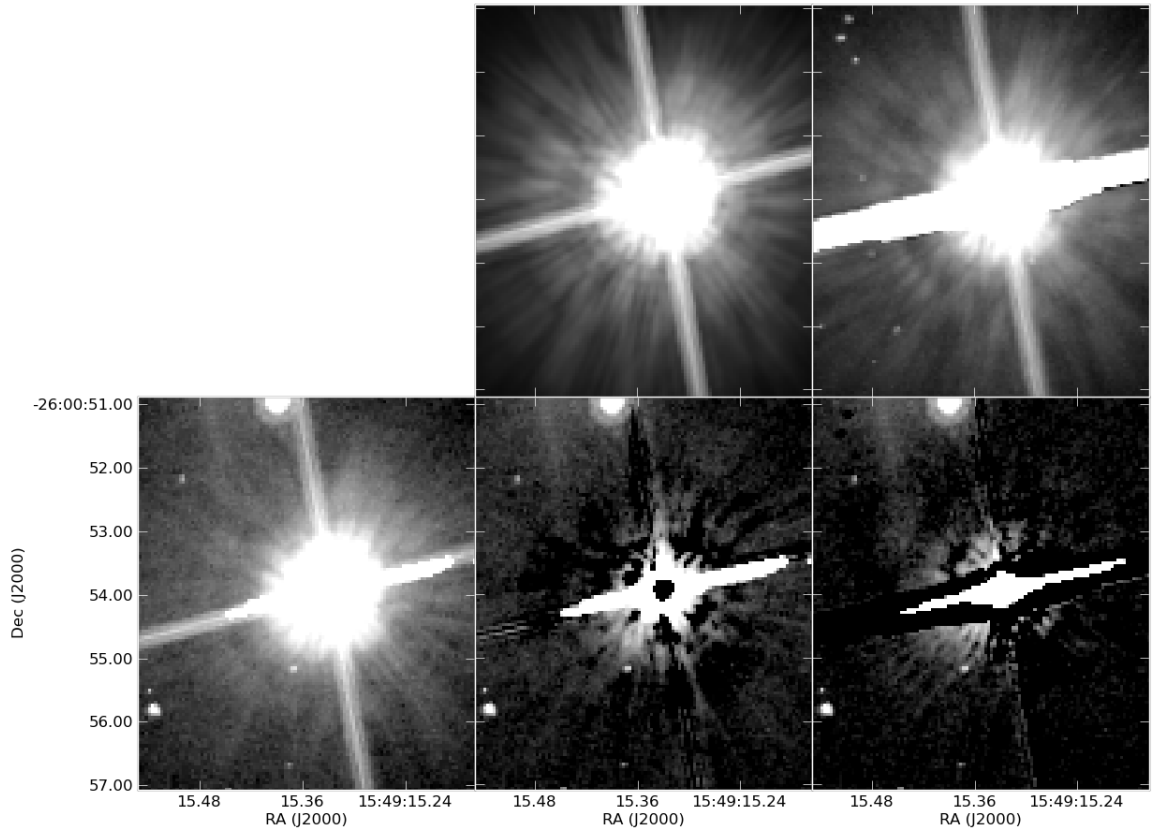

Fig. 5.— PSF subtraction results for the F814W image. The leftmost picture is the unsubtracted image, followed by the Tiny Tim PSF above its subtraction, and the field star PSF and subtracted image.

The registration and subtraction are performed in the same way as for the other filters. The subtraction results are shown in Figures 4 and 5. As demonstrated by these images, all of the subtractions share a common region of high nebulosity. Since the disk can be clearly resolved, I do not use any other PSFs. Similarly, PSF subtraction is performed on the POL0S image, using Tiny Tim PSFs and archive stars, allowing the disk to be seen in a region similar to that in the F555W and F814W images (see Fig. 6). Figure 7 compares the F555W, F814W, and POL0S subtraction results.

2.4. PDS 144S Photometry

The photometry of PDS 144S is measured using the method of 144C. However, instead of finding the counts in the best signal to noise radius, I use a square region around the star, due to the large diffraction spikes. Accordingly, I correct for this aperture. Table 1 shows the results, and Figure 8 an SED. The SED has infrared excesses characteristic of circumstellar dust. Interestingly, the

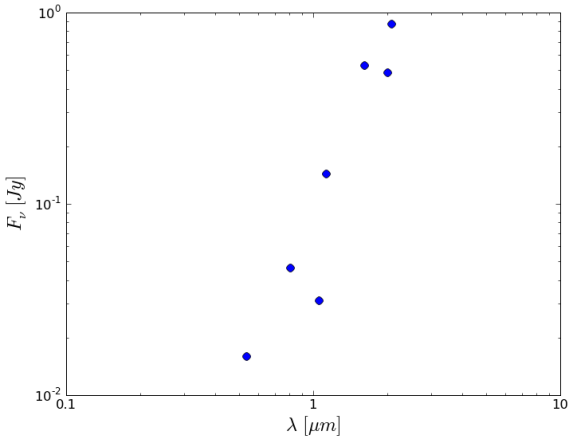

Fig. 8.— SED for PDS 144S.

two pairs of points which should have close to the same values do not. Specifically, the flux for the 2008 1.06 and 2 micron data is less than the flux for the 2006 1.12 and 2.06 micron data.

With a Python program, I measure the radial profile of the disk in the bands where it is visible. The star flux is taken into account by dividing the profile in each band by the flux of the star at that band (see Fig. 9). The ratio of the relative flux of the disk within a 1.05 arsecond radius at .5 microns to the relative flux at .8 microns is 2.2. The .8 micron to 1 micron ratio is 11.3. The ratios reveal the blue nature of the disk.

3. CONCLUSIONS

Performing photometry on PDS 144C, and comparing the resulting spectral energy distribution to model main sequence stars at the assumed distance of 140 parsecs, clearly demonstrates that that stars at this distance are not a good match to 144C. Furthermore, since adjusting the distance of these stars to obtain the best χ^2 value results in a best-fit value that is an order of magnitude larger than the assumed distance, I conclude that PDS 144C is not a part of the PDS 144 system.

The PSF subtractions for the .5, .8, and 1 micron images reveal a non-symmetric disk around PDS 144S. The disk is most visible in the .5 micron image, and with the disk radial profile, the conclusion that the disk is a blue disk can be drawn. The fact that the subtractions did not work at the other wavelengths attempted is consistent with the disk being blue.

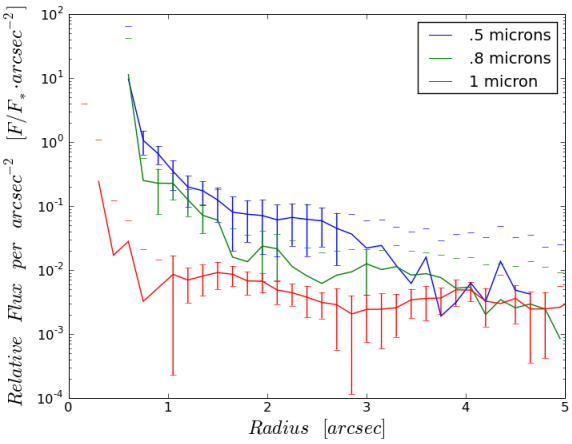

Fig. 9.— Radial profile for disk around PDS 144S.

REFERENCES

Grady, C. A., Harding, M., Bonfield, D., Hilton, G., Woodgate, B., Perrin, M., Melis, C., Peek, K., Smarr, O., Wisniewski, J., Schneider, G., Hines, D., Stapelfeldt, K., & Padgett, D. 2009, in Bulletin of the American Astronomical Society, Vol. 41, Bulletin of the American Astronomical Society, 224–+

Monin, J.-L., Clarke, C. J., Prato, L., & McCabe, C. 2007, in Protostars and Planets V, ed. B. Reipurth, D. Jewitt, & K. Keil, 395–409

Perrin, M. D., Duchêne, G., Kalas, P., & Graham, J. R. 2006, ApJ, 645, 1272

Vieira, S. L. A., Corradi, W. J. B., Alencar, S. H. P., Mendes, L. T. S., Torres, C. A. O., Quast, G. R., Guimarães, M. M., & da Silva, L. 2003, AJ, 126, 2971

Zuckerman, B. 2001, ARA&A, 39, 549

This work was supported by the National Science Foundation through the Research Experience for Undergraduates program.

This 2-column preprint was prepared with the AAS LaTeX macros v5.2.

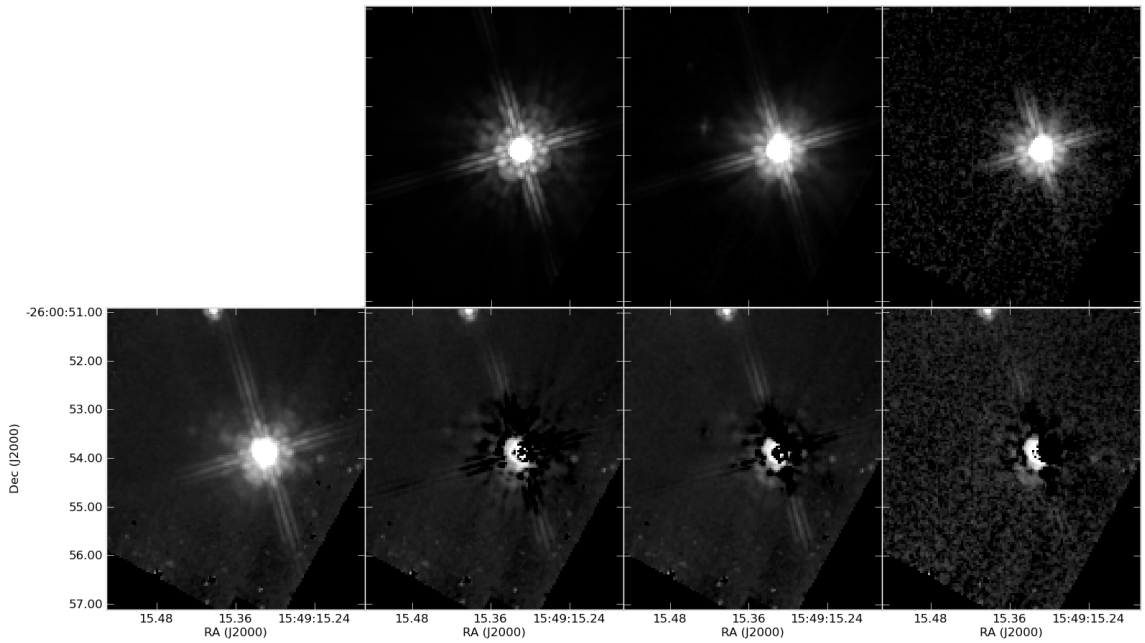

Fig. 6.— PSF subtraction results for the POL0S image. The leftmost picture is the unsubtracted image, followed by the Tiny Tim PSF above its subtraction, and two archive PSFs and their subtracted images.

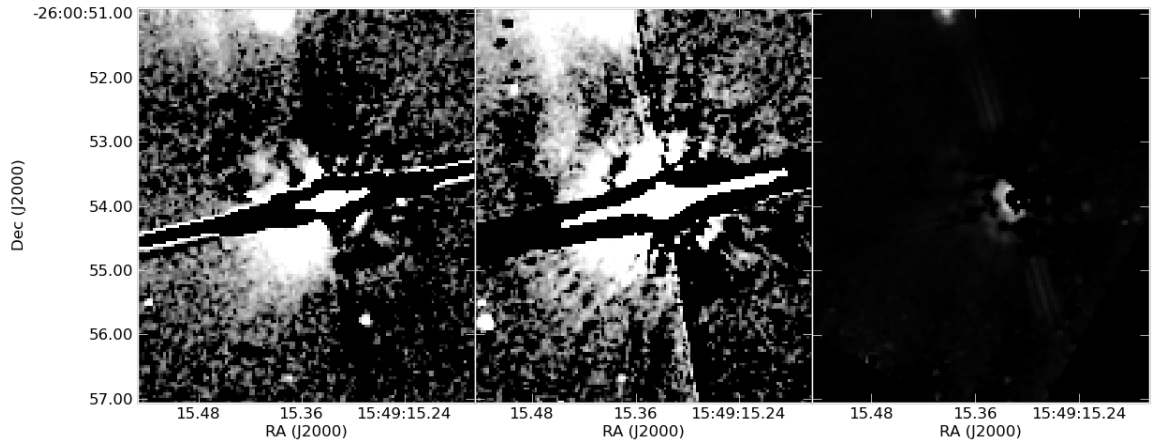

Fig. 7.— Comparison of the PSF subtractions for the F555W, F814W, and POL0S images. The images, from left to right, are the field star F555W subtraction, the field star F814W subtraction, and one of the POL0S subtractions performed with an archive PSF.